

PHOTOMASK

BACUS—The international technical group of SPIE dedicated to the advancement of photomask technology.

Experimental characterization of model resist materials

Oleg Kostko, Center for X-Ray Optics, Lawrence Berkeley National Laboratory, Berkeley, CA 94720, USA, Chemical Sciences Division, Lawrence Berkeley National Laboratory, Berkeley, CA 94720, USA; **Terry R. McAfee**, Center for X-Ray Optics, Lawrence Berkeley National Laboratory, Berkeley, CA 94720, USA; **Jonathan Ma**, Center for X-Ray Optics, Lawrence Berkeley National Laboratory, Berkeley, CA 94720, USA, Department of Physics, University of California, Berkeley, CA 94720, USA; **Patrick Naulleau**, Center for X-Ray Optics, Lawrence Berkeley National Laboratory, Berkeley, CA 94720, USA; **James M. Blackwell**, Components Research, Intel Corporation, Hillsboro, OR 97201, USA

ABSTRACT

New resists are needed to advance EUV lithography. The tailored design of an efficient photoresist is impossible without a fundamental understanding of EUV-induced chemistry. The absorption of a EUV photon by a thin film resist leads to the emission of primary and secondary electrons. The electrons may travel up to tens of nanometers before losing their kinetic energy via collisions which initiate chemical reactions. The “blur” of an aerial image is directly related to the distance that electrons can travel and initiate chemistry in the resist. Thus, identifying how to measure and influence the absorption of EUV photons, emission of electrons, and distance traveled by the secondary electrons is extremely beneficial to the resist community.

In this work, we present several experimental techniques to probe model polymer materials to investigate the impact of specific chemical groups on three critical resist properties: EUV absorption, electron emission, and electron attenuation length (EAL). EUV absorption dictates the efficiency of the film to absorb photons. Total electron yield (TEY) provides information on the conversion of absorbed EUV photons to electrons, whereas photoelectron spectroscopy (PES) provides information on the energies and abundance of generated electrons. The EAL corresponds to the thickness of a material required to reduce the number of emitted electrons to $1/e$ of the initial value. The EAL reveals the distance the electrons can travel in a resist film, which is directly related to the electron blur. Correlations between the obtained experimental values are discussed.

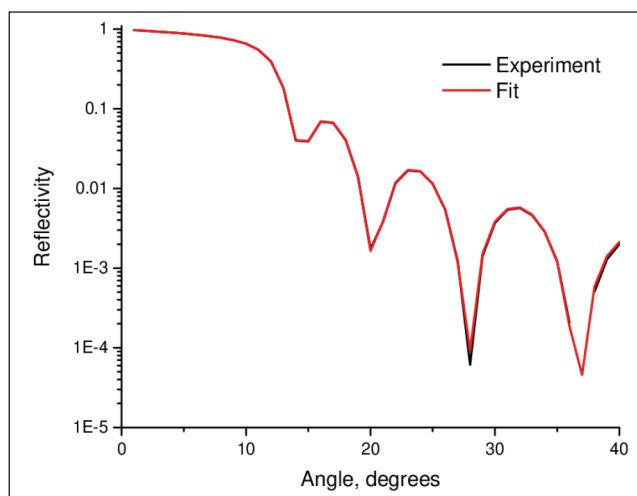


Figure 1. The experimental spectrum of reflectivity vs. angle (black line) and fit of the experimental data (red line) for polystyrene.

BACUS

N • E • W • S

SEPTEMBER 2022
VOLUME 38, ISSUE 9

SPIE/BACUS Scholarship recipient



Congratulations to **Bin Wang**, student at University of Colorado Boulder, for earning the 2022 SPIE-BACUS Scholarship.

The 2023 scholarship application will open in Spring 2023.

TAKE A LOOK INSIDE:

INDUSTRY BRIEFS
—see page 11

CALENDAR
For a list of meetings
—see page 12

SPIE.

EDITORIAL

High-NA EUV Lithography Challenges: Part I

Henry Kamberian, Photronics, Inc.

I attended this year's SPIE Advanced Lithography conference in San Jose, California, and the latest ASML technology conference in Veldhoven, Netherlands. After more than two years of hiatus from in-person conferences due to the Covid 19 pandemic, it was refreshing to finally see old friends (no offense to us aging engineers!) and again meet with industry colleagues.

From these two conferences, one important topic for me was the status of High-NA EUV technology.

We all know ASML has been developing the High-NA EUV lithography platform for some time. Based on today's EUV scanners with 0.33NA optics, the High-NA EUV platform is a completely new system, featuring 0.55NA optics, which enables scaling down to 8nm half-pitch resolution and below.

For all updates, installation of the first High-NA systems are expected in 2023 with volume manufacturing to start in 2025.

While some may consider the transition to High-NA EUV to be less drastic than the initial introduction of EUV lithography, most, as I do, believe this transition will bring significant changes in the EUV lithography ecosystem, especially to the EUV mask. Therefore, as mask makers, are we ready to meet the challenge of High-NA EUV at these aggressive timelines?

The 0.55NA is achieved through anamorphic projection optics. The anamorphic optics requires a change in mask-to-wafer reduction factor to 8x in scan direction and 4x in the other direction. Although the increase in image magnification 8x improves resolution with a reduction of shadowing effects, the drawback to the anamorphic projection optics is it cuts the exposure field size by half. This reduction in field size by half will force lithographers to pattern large chips using two masks through mask stitching methodology, which brings additional complexity to the patterning process. A key question: are there proven solutions for stitching device critical features at half-field boundaries?

The large NA in the 0.55NA platform brings another important change where the EUV illumination incidence angle is lower. This lower angle worsens the mask 3D effect further degrading exposure image contrast. The simplest approach to lessening mask 3D effect would be to reduce the thickness of existing absorbers. However, the lower thickness limit for the current Ta-based absorbers are around 55nm due to an increase in the absorber's EUV reflectivity, which degrades the image contrast. As imaging features continue to shrink, this reinforces the need to change absorber materials. Novel absorber materials have been extensively studied and characterized over the past few years. Of the various novel absorbers, the low (n) absorber materials, classified as EUVPSM, have received the most attention and acceptance.

These two major changes to the current EUV mask lead to critical questioning and highlights the need for new solutions in key mask-making areas.

While these questions and possible solutions will be further discussed in Part II of this editorial, I would like to close, and keeping with Olympics closing ceremony tradition, call upon all youth (and aging) engineers of the world to assemble in Monterey, California on September 25 through 29 for the 2022 Photomask Technology and EUV Lithography conference. We should look forward to all High-NA EUV technology presentations and discussions at the conference, possibly gaining additional insight into new solutions or get our questions answered.



N • E • W • S

BACUS News is published monthly by SPIE for BACUS, the international technical group of SPIE dedicated to the advancement of photomask technology.

Managing Editor/Graphics Linda DeLano

SPIE Sales Representative, Exhibitions, and Sponsorships
Melissa Valum

BACUS Technical Group Manager Tim Lamkins

■ 2022 BACUS Steering Committee ■

President

Emily E. Gallagher, imec.

Vice-President

Kent Nakagawa, Toppan Photomasks, Inc.

Secretary

Jed Rankin, IBM Research

Newsletter Editor

Artur Balasinski, Infineon Technologies

2022 Photomask + Technology Conference Chairs

Bryan S. Kasprovicz, HOYA

Ted Liang, Intel Corp.

Members at Large

Frank E. Abboud, Intel Corp.

Uwe F. W. Behringer, UBC Microelectronics

Ingo Bork, Siemens EDA

Tom Cecil, Synopsys, Inc.

Brian Cha, Entegris Korea

Aki Fujimura, D2S, Inc.

Jon Haines, Micron Technology Inc.

Sungmin Huh, Samsung

Koji Ichimura, Dai Nippon Printing Co., Ltd.

Henry Kamberian, Photronics, Inc.

Romain J Lallement, IBM Research

Khalid Makhamreh, Applied Materials, Inc.

Jan Hendrik Peters, bmbg consult

Douglas J. Resnick, Canon Nanotechnologies, Inc.

Thomas Scheruebl, Carl Zeiss SMT GmbH

Ray Shi, KLA Corp.

Thomas Struck, Infineon Technologies AG

Anthony Vacca, Automated Visual Inspection

Vidya Vaenkatesan, ASML Netherlands BV

Andy Wall, HOYA

Michael Watt, Shin-Etsu MicroSi Inc.

Larry Zurbrick, Keysight Technologies, Inc.

SPIE.

P.O. Box 10, Bellingham, WA 98227-0010 USA

Tel: +1 360 676 3290

Fax: +1 360 647 1445

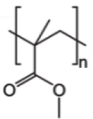
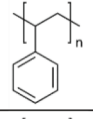
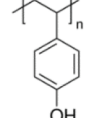
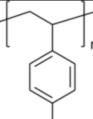
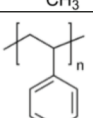
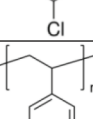
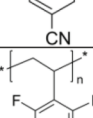
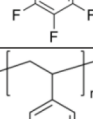
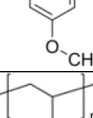
SPIE.org

help@spie.org

©2022

All rights reserved.

Table 1. Selected polymers, structure, chemical characterization, and EUV photoabsorption cross-section of monomers.

Material	Structure	Formula	M , g/mol	M_n $\times 10^3$	PDI	σ , Mb
poly(methyl methacrylate)		$C_5H_8O_2$	100.12	$M_w = 15,000$		7.30
polystyrene		C_8H_8	104.15	10	1.35	4.84
poly(4-hydroxystyrene)		C_8H_8O	120.15	$M_w = 11,000$		6.94
poly(4-methylstyrene)		C_9H_{10}	118.18	8.2	1.05	5.47
poly(4-chlorostyrene)		C_8H_7Cl	138.60	9.5	1.15	5.94
poly(4-cyanostyrene)		C_8H_7N	129.16	20.5	1.48	6.61
poly(pentafluorostyrene)		$C_8H_3F_5$	194.10	6	1.3	20.92
poly(4-methoxystyrene)		$C_9H_{10}O$	134.18	9.5	1.2	7.57
poly(4-acetoxystyrene)		$C_{10}H_{10}O_2$	162.19	10.5	1.6	10.25

1. Introduction

In Extreme Ultraviolet (EUV) lithography, only a small fraction of EUV (92 eV) photons are absorbed by a resist film. About 10%–30% of EUV photons can be absorbed by a 30 nm thick film, depending on the film composition.¹ The remaining EUV radiation will be absorbed by a substrate or an underlayer below the resist film. Absorption of a EUV photon by either of them will cause the emission of a photoelectron. The emitted electron can inelastically scatter and generate several slow secondary

electrons. Considering the multiplicative nature of slow electron generation, EUV resists should be tuned to capitalize on the abundance of slow electrons to initiate chemical transformations that eventually lead to pattern formation. Therefore, it is very important to understand all processes initiated by electron–resist interactions as well as the length scale on which the electrons can propagate upon ionization. This length scale will ultimately define the resolution of EUV lithography.

In this work, we utilize several model polymer materials to investigate the impact of specific chemical groups on the properties of those materi-

Table 2. Calculated and measured linear and mass attenuation coefficients for investigated polymers.

Material	Density, g/cm ³	β	Measured μ , μm^{-1}	Calculated μ , μm^{-1}	Measured μ/ρ , cm ² /g	Calculated μ/ρ , cm ² /g
poly(methyl methacrylate)	1.180	0.00587	5.46	5.18	46,310	43,892
polystyrene	1.000	0.00291	2.71	2.80	27,120	28,009
poly(4-hydroxystyrene)	1.160	0.00419	3.90	4.04	33,612	34,791
poly(4-methylstyrene)	1.040	0.00286	2.66	2.90	25,608	27,897
poly(4-chlorostyrene)	1.220	0.00320	2.97	3.15	24,378	25,817
poly(4-cyanostyrene)	1.075	0.00358	3.34	3.31	31,030	30,811
poly(pentafluorostyrene)	1.406	0.01823	16.97	9.13	120,684	64,902
poly(4-methoxystyrene)	0.962	0.00390	3.63	3.27	37,709	33,983
poly(4-acetoxystyrene)	1.060	0.00464	4.32	4.03	40,784	38,058

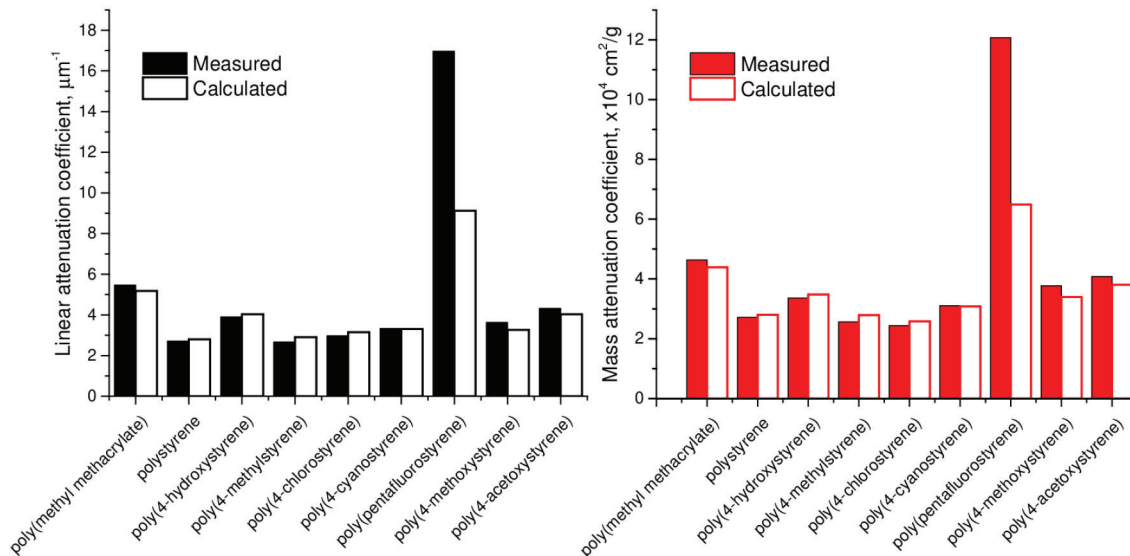


Figure 2. Left panel: Experimental values of EUV linear attenuation coefficient (filled columns) compared with calculated values, shown as non-filled columns. Right panel: The same for mass attenuation coefficient.

als to absorb EUV photons, generate electrons after EUV absorption, and transport the generated electrons. For this, several types of measurement are performed on the model polymers, including EUV absorption, total electron yield (TEY), electron attenuation length (EAL), and photoelectron spectroscopy (PES). The EUV absorption measurement characterizes the efficiency of material to capture EUV photons, which are needed to start the lithography process. TEY determines the number of electrons escaping from the film after EUV photon absorption. That number is proportional to the number of electrons generated by EUV radiation inside of the film. Together with EUV absorption measurement, it allows for the evaluation of the EUV photon to the electron conversion efficiency of a particular material. The EAL measurement characterizes distances which slow electrons can travel in a resist film, the value is directly related to the resolution of final photoresists. Photoelectron spectroscopy provides information not only on the abundance of emitted electrons but also on their energies, allowing for the characterization of the energy distribution of EUV-generated electrons.

2. Choice of Materials

We plan to systematically investigate the above-mentioned properties

of EUV resist materials, starting from building blocks of the photoresists (polymers, photoacid generators (PAGs), etc.), and moving to composite materials. Such an approach will help with understanding the function of each resist component and its role in a complex resist concoction. A set of the model, polystyrene-based polymers, as well as poly (methyl methacrylate) (PMMA), were chosen to investigate how different functional groups affect their properties. Materials were obtained from commercial suppliers and used without further purification. The density of polymers was obtained from literature sources.

3. Reflectometry

To obtain EUV absorption properties of materials two approaches are used: experimental determination and calculations. The measurement of absorption was performed at the Advanced Light Source (ALS) at Lawrence Berkeley National Laboratory using the reflectivity method. In this approach, the reflectivity at 13.5 nm from the thin polymer films was measured as a function of the angle. The example of experimental data for polystyrene is presented in Figure 1.

From the observed in the experiment behavior the components of complex refractive index n can be obtained:

Table 3. Experimental values of total electron yield, electron attenuation length, and Hammett para- substituent constants σ_p .

Material	TEY, 10^{-5} a.u.	EAL, nm	σ_p
poly(methyl methacrylate)	11.49±0.57	2.15±0.10	—
polystyrene	6.15±0.31	—	0.00
poly(4-hydroxystyrene)	7.06±0.35	1.47±0.10	-0.37
poly(4-methylstyrene)	6.32±0.32	—	-0.17
poly(4-chlorostyrene)	4.99±0.25	1.35±0.20	0.23
poly(4-cyanostyrene)	9.94±0.50	—	0.66
poly(pentafluorostyrene)	15.42±0.77	1.29±0.10	0.06 (0.34)*
poly(4-methoxystyrene)	7.95±0.40	2.00±0.15	-0.27
poly(4-acetoxystyrene)	8.30±0.42	1.78±0.10	0.31 ⁵ or -0.02 ⁶

*Constant for meta- substitution

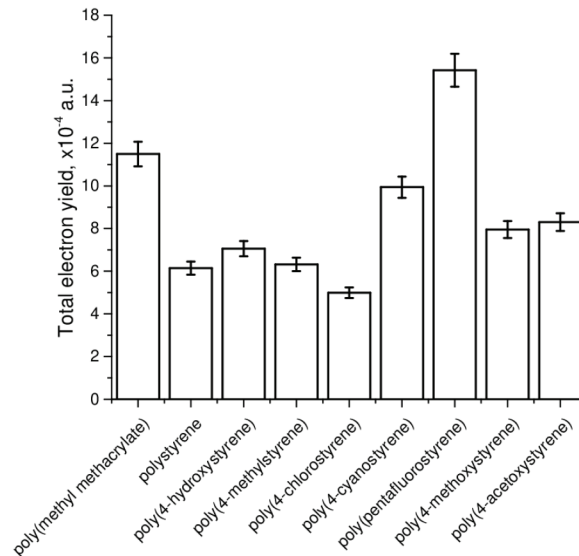


Figure 3. Total electron yield values for studied polymers.

$$n = 1 - \delta + i\beta, \quad (1)$$

where δ is dispersive and β is absorptive components of the refractive index of the polymer film. The imaginary part β of the refractive index can be obtained by fitting the experimental data as shown in Fig. 1.² From the obtained value of β , the linear attenuation coefficient μ of the polymer can be calculated by using Eq. (2):

$$\mu = \frac{\rho N_A}{M} \sigma = \frac{4\pi}{\lambda} \cdot \beta, \quad (2)$$

where ρ is the density, N_A is the Avogadro constant, M is the molar mass of a molecule, σ is the photoabsorption cross-section of a molecule, calculated using experimental atomic photoabsorption cross-sections from the CXRO X-ray database,^{3,4} and λ is the irradiation wavelength.

The mass attenuation coefficient μ/ρ is thus

$$\frac{\mu}{\rho} = \frac{N_A}{M} \sigma = \frac{4\pi}{\lambda \rho} \cdot \beta. \quad (3)$$

Both calculated and experimental linear and mass attenuation coefficients are summarized in table 2 and Fig. 2. A good correlation between the experimental and calculated values is observed. For poly(pentafluorostyrene) a big discrepancy between the measured and calculated values is noticed. During the measurement of that sample, it was observed that repeated measurements of the sample were not identical, suggesting sample degradation during the measurement.

From the analysis of tables 1 and 2 and figure 2, it is apparent that the addition of oxygen or fluorine leads to higher EUV absorption. Also, more dense materials have better absorption than the less dense in the case that their monomers have the same photoabsorption cross-section. Two notable cases are poly (methyl methacrylate) and poly(4-methoxystyrene). Both have comparable cross-sections of monomers (7.30 Mb and 7.57 Mb, correspondingly), but PMMA has better linear and mass attenuation coefficients due to its 23% higher density.

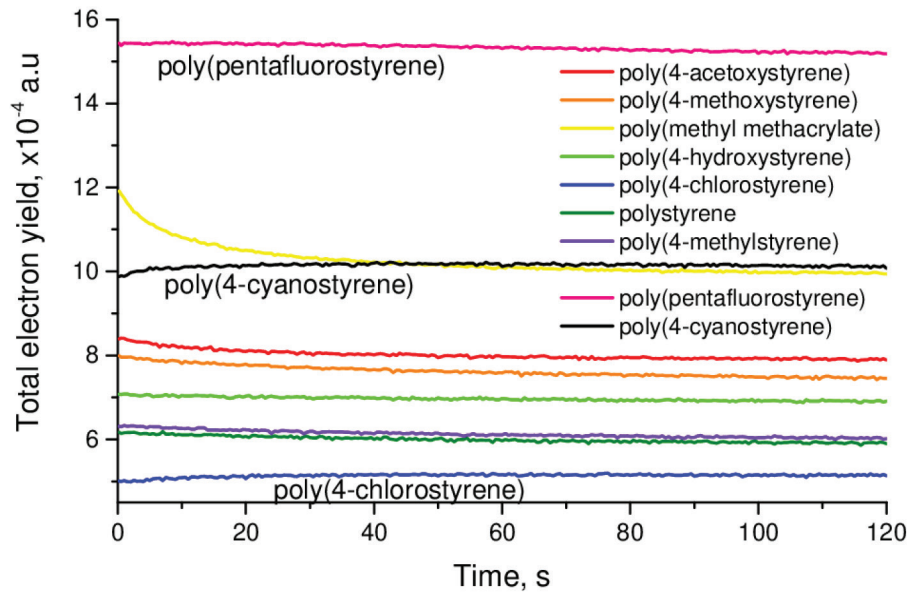


Figure 4. Time dependence of TEY signal for different materials. EUV dose is about $5 \text{ mJ}/(\text{cm}^2 \cdot \text{s})$.

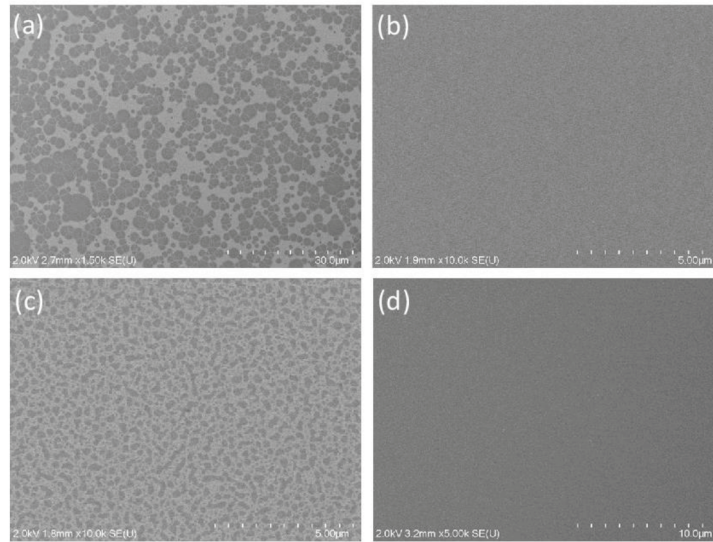


Figure 5. SEM images of films thinner than 5 nm of poly(4-chlorostyrene) are shown in (a) and (b), and poly (pentafluorostyrene) in (c) and (d). (a) and (c) are examples of poor-quality films while (b) and (d) are examples of good-quality films.

4. Total Electron Yield

To measure the total electron yield, the drain current was measured as a function of time. Apart from the properties of the material, the incident photon flux would also affect the drain current. Beamline conditions vary from one experiment to another, resulting in changes in photon flux. To meaningfully compare multiple samples, one measures the electron yield per unit of photon flux. Therefore, prior to each experiment, the photon flux is measured with a silicon diode and the drain current data is normalized with the diode current. ALS storage ring current fluctuations would manifest as fluctuations in flux. The storage ring current is therefore measured concurrently with both diode and drain current measurements to mitigate this problem.

As most samples are to a certain extent sensitive to EUV radiation, only the measurements when EUV exposure of samples just started ($t = 0\text{s}$) are representative of a sample in its original state. However, measuring only one data point would make the experiment very sensitive to noise. Moreover, as we would explain later, the time dependence could provide useful information about the materials.

To reduce the uncertainty in the TEY intensity at $t = 0\text{s}$ (I_0), we fit the TEY time evolution with a simple model assuming there are three components. The model value of I_0 essentially uses information from neighboring data points to mitigate the uncertainty of a single data point measurement.

$$I(t) = C_c + C_r \left[1 - \exp\left(-\frac{t}{t_r}\right) \right] + C_d \exp\left(-\frac{t}{t_d}\right) \quad (4)$$

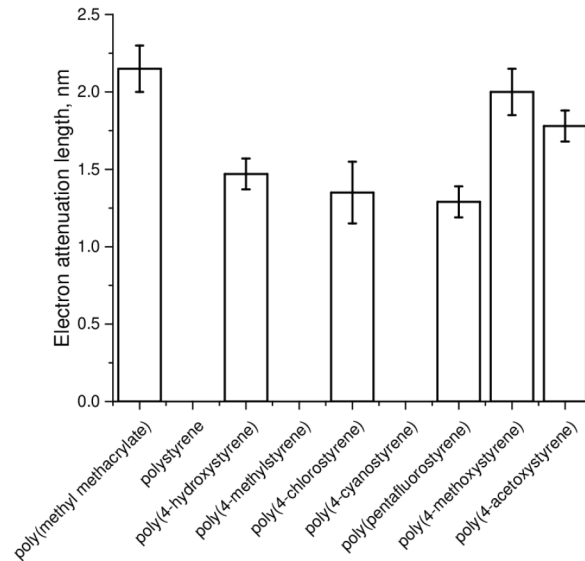


Figure 6. Experimental values of EAL in different polymer films.

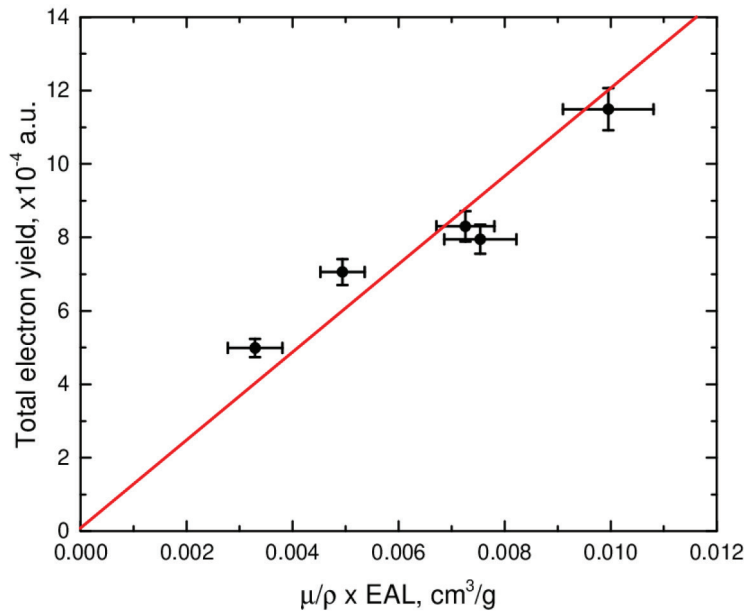


Figure 7. Total electron yield as a function of mass attenuation coefficient convoluted with EAL. A linear fit of the data is shown in red.

In equation (4), C_c is the constant component, C_r is the rising component, and C_d is the decaying component. To make error propagation more transparent, new variables are introduced to make I_0 itself a model parameter:

$$I_0 = C_c + C_d$$

$$r_r = \frac{C_r}{I_0}$$

$$r_d = \frac{C_d}{I_0}$$

As a result, equation (4) is rewritten:

(5)

$$\begin{aligned}
 I(t) &= I_0 - I_0 r_d + I_0 r_r \left[1 - \exp\left(-\frac{t}{t_r}\right) \right] + I_0 r_d \exp\left(-\frac{t}{t_d}\right) \\
 &= I_0 \left[1 - r_d + r_r \left[1 - \exp\left(-\frac{t}{t_r}\right) \right] + r_d \exp\left(-\frac{t}{t_d}\right) \right] \\
 &= I_0 \left[1 + r_r \left[1 - \exp\left(-\frac{t}{t_r}\right) \right] + r_d \left[\exp\left(-\frac{t}{t_d}\right) - 1 \right] \right]
 \end{aligned}
 \tag{6}$$

All data traces are therefore fitted against equation (6) to extract I_0 and its uncertainty. We note that the current uncertainty ceiling inferred from reproducibility is around 5%, which is way above the usual fitting uncertainty. The extracted I_0 values are summarized in Table 3 and shown

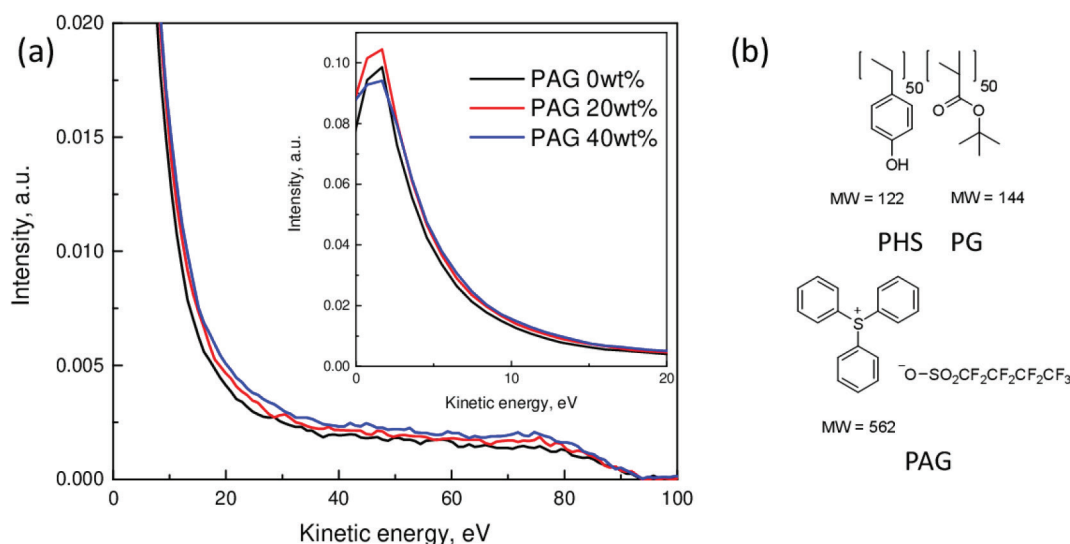


Figure 8. (a) Photoelectron spectra of polymer with three different PAG loadings. (b) Chemical structures of polymer matrix and PAG. PHS – poly (4-hydroxystyrene), PG – protective group, PAG – photoacid generator.

in Fig. 3.

One may observe a correlation between the TEY intensity at $t = 0$ s and the EUV attenuation properties, Figs. 3 and 2, correspondingly. Indeed, the EUV photons should be absorbed by the sample to initiate electron emission. Part of the emitted electrons, leaving the sample surface is detected in the TEY experiment. While for most of the samples a correlation between TEY and μ/ρ is observed, poly (4-cyanostyrene) demonstrates a higher TEY than expected from mass attenuation coefficient, which is close to those of polystyrene or poly(4-methylstyrene).

In most samples, the rising component of TEY time dependence is negligible (Eq. 6), and there is an obvious decay on top of the constant component in those samples (see Fig. 4). There are a few possible reasons behind the decay. Firstly, materials can outgas during exposure, which is very evident in PMMA. PMMA is known to evolve CO_2 upon radiation.^{7,8} Since oxygen has stronger EUV absorption than carbon, the loss of EUV absorption is faster than the loss of density, resulting in the reduction of TEY. Secondly, sample charging due to the emission of electrons has been suggested. However, we report that if EUV is paused for 2 minutes after a 2-minute exposure, TEY would not recover after the pause. Instead, it continues the previous trend, suggesting the decaying component has chemical origins and is not due to sample charging.

With the introduction of electron-withdrawing groups such as the cyano-, chloro-, and fluoro- group, the rising component of (Eq. 6) becomes more prominent. Such functional groups tend to have higher electron affinity with some of them even capable of dissociative electron attachment. Prior to electron attachment, these groups increase the probability that the electrons are being captured. In other words, prior to EUV exposure, they increase the electron capturing cross-section. During exposure, secondary electrons are generated and absorbed by these groups. Since each group can only absorb a limited number of electrons, most likely one, they will be gradually saturated as the exposure proceeds. Some might even dissociate upon electron attachment. As a result, the electron capturing cross-section would decrease overexposure, allowing more electrons to escape, producing a rising component, as observed in Fig. 4.

5. Electron Attenuation Length

The experimental approach to determine electron attenuation length is described previously.⁹ Briefly, polymer films of different thicknesses (1-10

nm) were prepared by spin-coating on silicon wafers. The coupons, cut from the wafers, were illuminated to 200 eV X-rays, which mostly penetrate through the polymer film, but are absorbed by the silicon wafer. Part of the electrons, generated by X-rays in the wafer, penetrate through the polymer film. Measurement of the current, generated by electrons transmitted through the films of different thicknesses, allows for the determination of electron attenuation length – the thickness of resist material required to reduce the number of emitted secondary electrons to 1/e of the initial. The method assumes that most electrons leaving the Si wafer will be low kinetic energy secondary electrons, with energies below 20 eV. For the EAL measurement, it is also extremely critical to know the thickness of the films.

Achieving film uniformity is a challenge for films less than ~10 nm, yet film uniformity is critical to obtaining accurate EAL values for a material. The scanning electron microscopy (SEM) images shown in figure 5 provide two examples of poor-quality films alongside a good-quality film of the same material. The recipes used for all four films in Fig. 5 are remarkably similar, with just slight differences in solvent ratios and spin-coating duration. We found it to be critical to verify film quality with either SEM or atomic force microscope (AFM). Measuring the thickness of these films with ellipsometry is also more difficult than normal due to the degeneracy of the film thickness, the index of refraction of the film, as well as the thickness of the native oxide on the wafer. The index of refraction of the material and the thickness of the oxide layer need to be measured first from separate samples so that those parameters can be held constant when fitting for the film thickness.

If the thin films are not inspected using AFM or SEM, there could be errors in the determination of EAL. For example, the same film thickness could be measured by ellipsometer for both good and poor-quality films, such as shown in Fig. 5. While the good quality films will generate useful data for EAL determination electron signal, in the case of poor-quality films, most of the electrons will be released directly by regions of the substrate uncoated by the film. This may explain the somewhat poor exponential fit and high value of EAL in our previously reported determination of EAL for poly (4-hydroxystyrene).⁹

The experimental values of EAL in the polymer films are presented in Table 3 as well as in Figure 6. Most of the EAL values fall in a range between 1 and 2 nm with PMMA having the largest EAL value of 2.15 nm and poly (pentafluorostyrene) – having the smallest EAL of 1.29 nm.

As was discussed above for the case of the TEY time dependence, the electron-withdrawing groups in the case of poly (pentafluorostyrene) or poly (4-chlorostyrene) may lead to efficient electron capture and therefore lead to smaller values of EAL. A Hammett substituent constant is used to characterize electron donating or withdrawing properties of substituents. Thus, it will be instructive to compare the trend, observed for EAL with the Hammett parameter, which is summarized in table 3. While there is a correlation between the Hammett parameter and the EAL for chloro-, hydroxy-, and methoxy- substituted polystyrenes, the results are less clear for poly (pentafluorostyrene) and poly (4-acetoxystyrene). For the first one, the direct comparison is not viable because the fluorine group occupies not only para- but also meta- and ortho- positions. For the acetoxy- group two very different Hammett constants could be found: from very positive, electron-withdrawing,⁵ to slightly negative, electron-donating.⁶ We are planning to expand the EAL determination to the missing samples, which may clarify if there is a correlation between electron donating or withdrawing properties and the value of the EAL.

6. Correlation Between Measurements

Similarly, to the case of near edge X-ray absorption fine structure (NEXAFS) spectroscopy, the intensity of collected TEY signal is a function of the density (ρ_e) of electrons emitted after absorption of EUV photons and EAL, which defines the probability of electrons to escape from the sample and be detected in measurement.¹⁰ In the general case where EAL and internal electron spectrum are energy-resolved, one has the relation

$$TEY = \int_0^{92} \rho_e(E) dE \int_0^\infty e^{-z/EAL(E)} dz \quad (7)$$

where z is the depth below the sample surface.

However, since the substrate injected secondary electrons mostly have low kinetic energies,⁹ the experimentally measured EAL should be rather representative for them. Therefore, by defining $\int_0^{92} \rho_e(E) dE$ as the density of low kinetic energy electrons:

$$TEY = \rho_e \int_0^\infty e^{-z/EAL} dz = \rho_e \times EAL \quad (8)$$

Intuitively, higher volumetric EUV absorption would lead to higher electron density. Materials with a higher quantum efficiency (η) produce more electrons with one photon so ρ_e is also proportional to η , which means:

$$TEY \propto \mu \times \eta \times EAL \quad (9)$$

Assuming the same quantum efficiency for all studied materials (and for simplicity equal to unity) the dependence of TEY intensity as a function of $\mu/\rho \times EAL$ is presented in Fig. 7. For five materials the shown dependence has a linear behavior. Poly (pentafluorostyrene) was excluded from the comparison because its experimental EUV attenuation coefficient is unreliable.

We are planning to expand the study to other materials to determine if the observed linear correlation has a universal character applicable to all materials. In the analysis presented in Fig. 7, we also assumed that the quantum efficiency of all studied materials is the same, however, it can be different and, in the future, we are planning to explore the possibility to extract the quantum efficiency from the experimental data.

7. Photoelectron Spectroscopy

Photoelectron spectra collected from samples of polymer with different PAG loading are shown in Fig. 8a. The polymer matrix consists of a 1:1 random copolymer of 4-hydroxystyrene and t-butyl protected methacrylate monomer doped with triphenylsulfonium perfluoro-1-butanefosfonate used as PAG (Fig. 8b). In the photoelectron spectra, one may see an intense and broad peak corresponding to slow electrons with kinetic energies below 20 eV and peaking around 2 eV. Above 20 eV the spectra are feature-less, and the signal goes to zero around 90 eV. In the photoelectron spectra, the high kinetic energy signal originates due to the

emission of primary, valence electrons after absorption of EUV photons. The fluorine atoms, included in PAG, may also emit electrons from the 2s shell at the lower kinetic energy of about 56 eV. Most of the electron signal below 60 eV is due to the emission of secondary electrons. Those electrons appear because of the inelastic scattering of primary electrons. There could be other, minor channels to generate secondary electrons, such as Auger electron emission.

One may see a very small difference between all three photoelectron spectra shown in Fig. 8a, with the signal between 20 to 80 eV slightly increasing with an increase of PAG loading. The total number of emitted electrons is increased by 10% for 20wt% PAG loading and by 9% for 40wt% PAG loading. To test if the increased electron emission is due to the enhanced EUV absorption, the mass attenuation coefficients were calculated for all three samples. The increased loading of PAG leads to the increase of the EUV absorption mostly due to the fluorine atoms in PAG. The calculated increase of EUV mass attenuation coefficient is 8% for 20wt% PAG and 13% for 40wt% PAG samples, which is close to what was observed in the experiment.

An interesting difference is observed for the high (40 wt.%) PAG loading sample. Firstly, in the experiment, we observe a smaller total number of emitted electrons than in the case of 20 wt% PAG, which is contradictory to the increased EUV absorption. Secondly, we observe a change in the distribution of slow vs. fast electrons. While both pure polymer matrix and 20 wt.% PAG sample has 81.9% and 81.4% of slow electrons (electrons with energy below 20 eV), correspondingly. Whereas the 40wt% PAG sample has 79.0% of slow electrons. This small decrease of the number of slow electrons, coupled with the smaller total number of electrons emitted from the sample could indicate that some electrons, generated by EUV exposure in the sample, can be trapped by the PAG.

8. Conclusions

We present the results of fundamental research of model polymers using several experimental techniques. We determined the absorption properties of these materials using reflectometry. The total electron yield measurement characterizes the property of the material to generate electrons after EUV absorption and the temporal evolution of the TEY signal provides information on electron capture by the material. For the same range of materials, we determined the average distance the emitted electrons can travel in the film, characterized by the EAL value. We also discuss the correlation between these three experimental values. The photoelectron spectra of the resist materials can provide information on the abundance and kinetic energies of electrons generated by EUV photons, as well as the ratio of slow vs. fast electrons. The demonstrated techniques will be applied to study more complex resist materials, such as complete resist systems and inorganic resist materials. The acquired data provides a new fundamental understanding of EUV-generated electrons which presumably can be leveraged for the development of better EUV resist materials.

9. Acknowledgements

We appreciate the assistance of Eric Gullikson during measurements and absorption data analysis and Luke Long for PES sample preparation. This work was supported by Intel and Samsung through the U.S. Department of Energy under Contract No. DE-AC02-05CH11231. This research used resources of the Advanced Light Source, a U.S. DOE Office of Science User Facility under contract no. DE-AC02-05CH11231.

10. References

- [1] Ogletree, D. F., "Molecular excitation and relaxation of extreme ultraviolet lithography photoresists," *Frontiers of Nanoscience* 11, 91-113 (2016).
- [2] Kwark, Y.-J., Bravo-Vasquez, J. P., Chandhok, M., Cao, H., Deng, H., Gullikson, E., and Ober, C. K., "Absorbance measurement of polymers at extreme ultraviolet wavelength: Correlation between experimental and theoretical calculations," *Journal*

of *Vacuum Science & Technology B: Microelectronics and Nanometer Structures Processing, Measurement, and Phenomena* 24(4), 1822-1826 (2006).

- [3] Henke, B. L., Gullikson, E. M., and Davis, J. C., "X-Ray Interactions: Photoabsorption, Scattering, Transmission, and Reflection at $E = 50\text{--}30,000$ eV, $Z = 1\text{--}92$," *At. Data Nucl. Data Tables* 54(2), 181-342 (1993).
- [4] Data from the Center for X-Ray Optics (CXRO) at Lawrence Berkeley National Laboratory, <https://henke.lbl.gov/>.
- [5] Hansch, Corwin., Leo, A., and Taft, R. W., "A survey of Hammett substituent constants and resonance and field parameters," *Chem. Rev.* 91(2), 165-195 (1991).
- [6] Papp, T., Kollár, L., and Kégl, T., "Employment of quantum chemical descriptors for Hammett constants: Revision Suggested for the acetoxy substituent," *Chemical Physics Letters* 588, 51-56 (2013).
- [7] Hiraoka, H., "Radiation Chemistry of Poly (methacrylates)," *IBM Journal of Research and Development* 21(2), 121-130 (1977).
- [8] Ennis, C. P. and Kaiser, R. I., "Mechanistical studies on the electron-induced degradation of polymethylmethacrylate and Kapton," *Phys. Chem. Chem. Phys.* 12(45), 14902-14915 (2010).
- [9] Ma, J. H., Naulleau, P., Ahmed, M., and Kostko, O., "Determination of effective attenuation length of slow electrons in polymer films," *Journal of Applied Physics* 127(24), 245301 (2020).
- [10] Stohr, J., [NEXAFS Spectroscopy], Springer Berlin Heidelberg (1996).



Sponsorship Opportunities

Sign up now for the best sponsorship opportunities

Photomask Technology + EUV Lithography 2022

Contact: Melissa Valum, Tel: +1 360 685 5596
melissav@spie.org

Advanced Lithography + Patterning 2023

Contact: Melissa Valum, Tel: +1 360 685 5445
melissav@spie.org or Kim Abair,
Tel: +1 360 685 5499, kima@spie.org

Advertise in the BACUS News!

The BACUS Newsletter is the premier publication serving the photomask industry. For information on how to advertise, contact:

Melissa Valum
Tel: +1 360 685 5596
melissav@spie.org

BACUS Corporate Members

Acuphase Inc.
American Coating Technologies LLC
AMETEK Precitech, Inc.
Berliner Glas KGaA Herbert Kubatz
GmbH & Co.
FUJIFILM Electronic Materials U.S.A., Inc.
Gudeng Precision Industrial Co., Ltd.
Halocarbon Products
HamaTech APE GmbH & Co. KG
Hitachi High Technologies America, Inc.
JEOL USA Inc.
Mentor Graphics Corp.
Molecular Imprints, Inc.
Panavision Federal Systems, LLC
Profilocolore Srl
Raytheon ELCAN Optical Technologies
XYALIS

Industry Briefs

■ Is There A Limit To The Number Of Layers In 3D-NAND?

Karen Heyman, Semiconductor Engineering

Memory vendors are racing to add more layers to 3D NAND, a competitive market driven by the explosion in data and the need for higher-capacity solid state drives and faster access time. Micron already is filling orders for 232-layer NAND, and not to be outdone, SK Hynix announced that it will begin volume manufacturing 238-layer 512Gb triple-level cell (TLC) 4D NAND in the first half of next year. Perhaps even more significant, chipmakers say privately they will leverage industry learning about stacking NAND for 3D-ICs, which currently are in development.

"Moore's Law for processors has arguably been lagging the last few years, but is alive and well for NAND flash," said Ben Whitehead, technical product manager at Siemens EDA. "It's a good thing, because modern compute and networking have an insatiable appetite for fast storage."

<https://semiengineering.com/is-there-a-limit-to-the-number-of-layers-in-3d-nand/>

■ The Truth About SMIC's 7-nm Chip Fabrication Ordeal

Majeed Ahmad, Electronic Design News

Semiconductor Manufacturing International Corp. (SMIC) reaching the 7-nm chip fabrication process has been a jaw dropper. Still, while it's making headlines in the technology and trade media, it's critical to examine the true value of SMIC's so-called great leap forward. Can SMIC mass produce chips at its newly developed 7-nm node?

According to some industry observers, SMIC's 7-nm yields per wafer are in the range of 15%. That makes the chips manufactured at this process node very costly, around 10 times the market price of a chip manufactured at TSMC's 7-nm node. It's also worth noting that the crypto-miner chip known to have been manufactured at SMIC's 7-nm node features a highly parallel design, which implies lower complexity.

In the final analysis, SMIC's 7-nm story relates more to China's political cause of semiconductor self-sufficiency than market economics. At the same time, however, it's a quasi-7-nm chip manufacturing process that could become a stepping stone for a true 7-nm process node. Here, the missing link is ASML's EUV technology, currently banned for semiconductor fabs in China.

<https://www.edn.com/the-truth-about-smics-7-nm-chip-fabrication-ordeal/>

■ Mexico Joins the List of Nations Wanting to Lure Chipmakers

Dan Robinson, The Register

Mexico is the next country in line to offer incentives to tempt semiconductor manufacturers to set up shop and may be aiming to take advantage of the US desire to bring manufacturing closer to home. Both the US and the EU have this year unveiled strategies aimed at encouraging chip companies to on-shore semiconductor production and reduce the reliance of their economies on silicon imported from Asia, especially Taiwan.

Mexico is now hoping to take advantage of the US desire to bring chip manufacturing closer to home. As a neighbor of the American economy, the country is well-placed to take advantage of US investment, and has already seen many companies locate factories there, so adding semiconductor manufacturing to the mix might seem a logical step.

https://www.theregister.com/2022/08/22/mexico_joins_the_list_nations/

Join the premier professional organization for mask makers and mask users!

About the BACUS Group

Founded in 1980 by a group of chrome blank users wanting a single voice to interact with suppliers, BACUS has grown to become the largest and most widely known forum for the exchange of technical information of interest to photomask and reticle makers. BACUS joined SPIE in January of 1991 to expand the exchange of information with mask makers around the world.

The group sponsors an informative monthly meeting and newsletter, BACUS News. The BACUS annual Photomask Technology Symposium covers photomask technology, photomask processes, lithography, materials and resists, phase shift masks, inspection and repair, metrology, and quality and manufacturing management.

Individual Membership Benefits include:

- Subscription to BACUS News (monthly)
- Eligibility to hold office on BACUS Steering Committee

spie.org/bacushome

Corporate Membership Benefits include:

- 3-10 Voting Members in the SPIE General Membership, depending on tier level
- Subscription to BACUS News (monthly)
- One online SPIE Journal Subscription
- Listed as a Corporate Member in the BACUS Monthly Newsletter

spie.org/bacushome

C A L E N D A R

2022

✱ **SPIE Photomask Technology + Extreme Ultraviolet Lithography**
25-29 September 2022
Monterey, California, USA
www.spie.org/puv

✱ **SPIE Photonics Industry Summit**
21 September 2022
Washington DC, USA
www.spie.org/dce

2023

✱ **SPIE Advanced Lithography + Patterning**
26 February - 2 March 2023
San Jose, California, USA
www.spie.org/al

SPIE, the international society for optics and photonics, brings engineers, scientists, students, and business professionals together to advance light-based science and technology. The Society, founded in 1955, connects and engages with our global constituency through industry-leading conferences and exhibitions; publications of conference proceedings, books, and journals in the SPIE Digital Library; and career-building opportunities. Over the past five years, SPIE has contributed more than \$22 million to the international optics community through our advocacy and support, including scholarships, educational resources, travel grants, endowed gifts, and public-policy development. www.spie.org.

SPIE.

International Headquarters
P.O. Box 10, Bellingham, WA 98227-0010 USA
Tel: +1 360 676 3290
Fax: +1 360 647 1445
help@spie.org • spie.org

Shipping Address
1000 20th St., Bellingham, WA 98225-6705 USA

SPIE.EUROPE

2 Alexandra Gate, Ffordd Pengam, Cardiff,
CF24 2SA, UK
Tel: +44 29 2089 4747
Fax: +44 29 2089 4750
info@spieeurope.org • spieeurope.org

You are invited to submit events of interest for this calendar. Please send to lindad@spie.org.